GEOPHYSICS, VOL. 85, NO. 5 (SEPTEMBER-OCTOBER 2020); P. M57–M71, 19 FIGS., 3 TABLES.
10.1190/GEO2019-0625.1

Bayesian petroelastic inversion with multiple prior models

Dario Grana[1]

ABSTRACT

Bayesian methods are commonly used for geophysical inverse problems, such as seismic and rock-physics inversion, for the prediction of petroelastic properties. Bayesian inversion is based on Bayes' theorem and combines the information from a prior distribution and a likelihood function; in geophysical applications, the prior model generally includes the available geologic information about the model variables, whereas the likelihood includes the geophysical models that link the model to the data. The goal of Bayesian inversion is to estimate the posterior distribution of the model variables conditioned by the measured data. The focus is on the prior model and its parameters. Typically, the parameters of the prior distributions are assumed to be fixed, for example, the mean and standard deviation of the prior distribution of petroelastic properties in seismic inversion or the facies proportions and transition probabilities in facies classification. I have studied the posterior distribution of the model given the data in a Bayesian setting using multiple prior models. The posterior distribution is assessed by summing the contributions of all of the likelihood functions of the model given the data, using different sets of parameters, weighted by the probabilities of the parameters. I apply the mathematical formulation in different problems, including log-facies classification, seismic-facies classification, and petrophysical property prediction and using different methods for the prior model generation such as transition matrices, training images, and Gaussian mixture models with multiple modes. The results show that multiple prior models can match the data and that the uncertainty in the prior parameters should be accounted for in the posterior distribution of the reservoir properties.

INTRODUCTION

The Bayesian framework is generally considered the natural approach for the geophysical inverse problem to predict a set of model variables from measured data sets and quantify their uncertainty (Tarantola, 2005). The inverse problem solution is the posterior distribution of the model variables conditioned by the measured data, at each location of the reservoir model.

Bayesian inverse theory has gained popularity in the geophysics community, and several applications to inversion of seismic data have been presented. Tarantola and Valette (1982) provide a general introduction to nonlinear geophysical inverse problems and their probabilistic formulation. Doyen (1988), Bortoli et al. (1993), and Haas and Dubrule (1994) present the first geostatistical methods for inversion of seismic data for petrophysical property estimation. An overview of Bayesian inverse theory, uncertainty quantification, and stochastic sampling algorithms for geophysical inverse problems is presented in Sen and Stoffa (1996) and Ulrych et al. (2001). Mukerji et al. (2001) and Eidsvik et al. (2004) combine Bayesian inversion with statistical rock physics in probabilistic seismic inversion methods. Buland and Omre (2003) propose an analytical solution of the Bayesian formulation of the linearized amplitude variation with offset inversion. Several subsequent works combine Bayesian inversion formulation with rock physics models to predict the probability distribution of petrophysical properties given seismic data as in Contreras et al. (2005), Gunning and Glinsky (2007), Spikes et al. (2008), Grana and Della Rossa (2010), Rimstad et al. (2012), Azevedo et al. (2013), Kemper and Gunning (2014), and Grana et al. (2017). These publications differ for the model variables (either discrete properties, such as facies, or continuous variables, such as petroelastic properties), the statistical assumptions (e.g., Gaussian, Gaussian mixture, generalized Gaussian or nonparametric probability density functions), the computational algorithms (analytical solutions versus Monte Carlo methods), and the physical models

Manuscript received by the Editor 20 September 2019; revised manuscript received 21 April 2020; published ahead of production 10 June 2020; published online 26 June 2020.
[1]Department of Geology and Geophysics, School of Energy Resources, University of Wyoming, Laramie, Wyoming 82071, United States. E-mail: dgrana@uwyo.edu (corresponding author).

(linearized or nonlinear seismic and rock physics operators). Bosch et al. (2010) provide an overview of the state of the art of petrophysical modeling and seismic reservoir characterization. Monte Carlo methods for stochastic sampling of elastic and petrophysical properties conditioned by seismic data have been proposed in Mosegaard and Tarantola (1995), Mosegaard (1998), Connolly and Hughes (2016) and de Figueiredo et al. (2019a, 2019b). The Bayesian formulation has also been applied to joint seismic and electromagnetic inversion (Chen et al., 2007).

In most applications, the prior model parameters are inferred from well logs and are assumed to be known in the inversion. The influence of the prior model in probabilistic inversion for geophysical inverse problems is discussed in Scales and Tenorio (2001). Sensitivity analyses on the prior models have been previously presented for several geophysical applications (Oldenburg and Li, 1999; Miller and Routh, 2007). Here, I propose to use multiple prior models and compute the posterior distribution by calculating the contribution of all the likelihood functions weighted by the probability of the model parameters and integrating over all possible prior parameters. By sampling from multiple prior models with different parameters, we generate several realizations and verify if the prior model parameters used to generate the realizations are consistent with the observed data. A prior falsification approach using multipoint geostatistics prior models for reservoir characterization has been presented by Park et al. (2013) and Scheidt et al. (2015, 2018). In their approach, the likelihood of different training images of generating the measured data is preliminarily computed, to reduce the number of prior models to be evaluated in the inversion.

In the proposed approach, I assume a set of plausible prior models based on geologic information or data from nearby wells (e.g., the transition probabilities of a first-order Markov chain or training images of a facies sequence), I sample the model parameters from the prior and compute a set of model realizations (e.g., the facies profiles at the well location), evaluate the likelihood of the measured data given the model realization, and finally compute the posterior distribution of the model given the data by summing all of the likelihood functions of the data given the model weighted by the prior probabilities.

In the "Application" section, I present five examples to illustrate the methodology and show the value of the prior distribution in the inversion including a real data application to well log data inversion for the prediction of facies and petrophysical properties. Examples 1 and 2 illustrate a facies classification problem for an alternating sequence of sand and shale, using synthetic seismic data. These examples are used to validate the methodology for different geostatistical simulation methods: Markov chain models and multipoint geostatistics. Example 3 shows a rock physics inversion of real well log data for petrophysical property prediction using multimodal distributions. This example shows the applicability to continuous variables such as petrophysical properties. Example 4 extends the previous example to joint facies and petrophysical properties prediction based on seismic data. Example 5 is a 2D application representing a vertical section of a clastic reservoir with three lithofluid facies.

METHODOLOGY

The focus of geophysical inverse problems is to predict the model variables $\boldsymbol{m}$ from measured data $\boldsymbol{d}$ assuming that the geophysical relations $\boldsymbol{g}$ that predicts the geophysical response of a given model is known as

$$\boldsymbol{d} = \boldsymbol{g}(\boldsymbol{m}) + \boldsymbol{e}, \tag{1}$$

where $\boldsymbol{e}$ is the error in the measurements. In seismic reservoir characterization, the geophysical relations $\boldsymbol{g}$ can include rock physics models such as granular media, inclusion, and empirical models (Mavko et al., 2009) to link petrophysical properties to elastic attributes (e.g., porosity and saturation to velocity and density) and seismic models such as Kennett's invariant imbedding method or linearized approximations based on convolution and Zoeppritz equations (Aki and Richards, 1980; Kennett, 1984; Tromp and Snieder, 1989; Mukerji et al., 1997) to link elastic attributes to their seismic response. The goal is to assess the posterior distribution $p(\boldsymbol{m}|\boldsymbol{d})$ from the prior distribution $p(\boldsymbol{m})$ of the model variables and the likelihood function $p(\boldsymbol{d}|\boldsymbol{m})$ of the data given the model variables

$$p(\boldsymbol{m}|\boldsymbol{d}) = \frac{p(\boldsymbol{d}|\boldsymbol{m})p(\boldsymbol{m})}{p(\boldsymbol{d})}, \tag{2}$$

where the probability $p(\boldsymbol{d})$ of the data is a normalization constant.

The formulation in equations 1 and 2 can be applied to discrete and continuous random variables. In geophysical applications, examples of inverse problems with continuous random variables include elastic inversion of seismic data (to predict a set of elastic properties such as velocities or impedances) and petrophysical inversion of seismic data (to predict a set of petrophysical variables such as porosity and mineral volumes), whereas examples of inverse problems with discrete random variables include facies or rock-type classification of seismic data. Therefore, the model variable $\boldsymbol{m}$ can be discrete or continuous. In the discrete case, the prior model is a probability mass function, whereas, in the continuous case, the prior model is a probability density function.

The parameters $\boldsymbol{\theta}$ of the prior model are the parameters that control the prior knowledge about the model. Examples of parameters are facies transition matrix probabilities, facies proportions, training images, mean and variance of Gaussian prior distributions of continuous properties, and spatial correlation parameters of discrete or continuous properties. Generally, the parameters $\boldsymbol{\theta}$ of the model are fixed in Bayesian inversion. But there might be multiple values of the same parameter that leads to the same geophysical response of the model, that is, the same predicted data. If the parameters $\boldsymbol{\theta}$ are not fixed, Bayes' theorem in equation 2 can be rewritten as follows:

$$p(\boldsymbol{m}|\boldsymbol{d},\boldsymbol{\theta}) = \frac{p(\boldsymbol{d}|\boldsymbol{m},\boldsymbol{\theta})p(\boldsymbol{m}|\boldsymbol{\theta})}{p(\boldsymbol{d}|\boldsymbol{\theta})}, \tag{3}$$

where $p(\boldsymbol{d}|\boldsymbol{m},\boldsymbol{\theta})$ is the likelihood function and $p(\boldsymbol{m}|\boldsymbol{\theta})$ is the probability of the model given the set of parameters $\boldsymbol{\theta}$. The denominator $p(\boldsymbol{d}|\boldsymbol{\theta})$ is a normalizing constant that represents the likelihood of the vector of data $\boldsymbol{d}$ for all possible model configurations $\boldsymbol{m}$ generated from the given prior model $\boldsymbol{\theta}$.

The posterior distribution $p(\boldsymbol{m}|\boldsymbol{d})$ can then be obtained by integrating over all of the possible parameters $\boldsymbol{\theta}$:

$$p(\boldsymbol{m}|\boldsymbol{d}) = \int_{\boldsymbol{\Omega}_{\boldsymbol{\theta}}} p(\boldsymbol{m}|\boldsymbol{d},\boldsymbol{\theta})p(\boldsymbol{\theta}|\boldsymbol{d})d\boldsymbol{\theta}, \tag{4}$$

where $\boldsymbol{\Omega}_{\boldsymbol{\theta}}$ is the parameter space (Papoulis, 1984).

The conditional distributions $p(\boldsymbol{m}|\boldsymbol{d},\boldsymbol{\theta})$ and $p(\boldsymbol{\theta}|\boldsymbol{d})$ can be computed using Bayes' theorem (Anderson, 1984). The posterior distribution $p(\boldsymbol{m}|\boldsymbol{d})$ becomes

$$p(\boldsymbol{m}|\boldsymbol{d}) = \int_{\boldsymbol{\Omega}_\theta} \frac{p(\boldsymbol{d}|\boldsymbol{m},\boldsymbol{\theta})p(\boldsymbol{m}|\boldsymbol{\theta})}{p(\boldsymbol{d}|\boldsymbol{\theta})} \frac{p(\boldsymbol{d}|\boldsymbol{\theta})p(\boldsymbol{\theta})}{p(\boldsymbol{d})} d\boldsymbol{\theta},$$
$$= \int_{\boldsymbol{\Omega}_\theta} \frac{p(\boldsymbol{d}|\boldsymbol{m},\boldsymbol{\theta})p(\boldsymbol{m}|\boldsymbol{\theta})p(\boldsymbol{\theta})}{p(\boldsymbol{d})} d\boldsymbol{\theta}. \quad (5)$$

If $\boldsymbol{\theta}$ is a continuous parameter, the integral in equation 5 must be approximated using numerical methods. Generally, it is necessary to discretize the parameter space $\boldsymbol{\Omega}_\theta$ such that it only includes a finite number of values. In geophysical applications, a further reduction of the parameter space $\boldsymbol{\Omega}_\theta$ can be obtained from prior geologic information, by imposing constraints on facies transitions and continuous properties bounds. For example, some facies sequences could be excluded if they do not represent geologically meaningful stratigraphy or violate depositional rules. If $\boldsymbol{\Omega}'_\theta$ indicates the reduced parameter space, equation 5 can be rewritten in the discrete formulation as

$$p(\boldsymbol{m}|\boldsymbol{d}) = \sum_{\boldsymbol{\Omega}'_\theta} \frac{p(\boldsymbol{d}|\boldsymbol{m},\boldsymbol{\theta})p(\boldsymbol{m}|\boldsymbol{\theta})p(\boldsymbol{\theta})}{p(\boldsymbol{d})}. \quad (6)$$

In the proposed approach, I first sample the model parameters from $p(\boldsymbol{\theta})$; I compute the model realizations from $p(\boldsymbol{m}|\boldsymbol{\theta})$; I develop the likelihood $p(\boldsymbol{d}|\boldsymbol{m},\boldsymbol{\theta})$ of the data given the model realizations and the parameters using the geophysical forward operator $\boldsymbol{g}$ in equation 1 (e.g., a rock-physics relation combined with a seismic wave propagation model); and I finally assess the posterior distribution $p(\boldsymbol{m}|\boldsymbol{d})$ using equation 6, which sums the contributions of all the likelihood $p(\boldsymbol{m}|\boldsymbol{d},\boldsymbol{\theta})$ weighted by the prior probability of the model and parameters $p(\boldsymbol{m},\boldsymbol{\theta}) = p(\boldsymbol{m}|\boldsymbol{\theta})p(\boldsymbol{\theta})$.

It is also possible to evaluate the posterior probability $p(\boldsymbol{\theta}|\boldsymbol{d})$ as

$$p(\boldsymbol{\theta}|\boldsymbol{d}) = \frac{p(\boldsymbol{d}|\boldsymbol{\theta})p(\boldsymbol{\theta})}{p(\boldsymbol{d})}, \quad (7)$$

to determine the set of prior parameters that most likely describe the measured data. The likelihood $p(\boldsymbol{d}|\boldsymbol{\theta})$ can be obtained by integration over all of the possible model realizations (Papoulis, 1984)

$$p(\boldsymbol{\theta}|\boldsymbol{d}) = \frac{p(\boldsymbol{\theta})}{p(\boldsymbol{d})} \int_{\boldsymbol{\Omega}_m} p(\boldsymbol{d}|\boldsymbol{m},\boldsymbol{\theta})p(\boldsymbol{m}|\boldsymbol{\theta})d\boldsymbol{m}, \quad (8)$$

where the domain $\boldsymbol{\Omega}_m$ is the space of the model realizations. The integral in equation 8 can be approximated using a finite sum over a discretized domain $\boldsymbol{\Omega}'_m$

$$p(\boldsymbol{\theta}|\boldsymbol{d}) = \frac{p(\boldsymbol{\theta})}{p(\boldsymbol{d})} \sum_{\boldsymbol{\Omega}'_m} p(\boldsymbol{d}|\boldsymbol{m},\boldsymbol{\theta})p(\boldsymbol{m}|\boldsymbol{\theta}). \quad (9)$$

Similarly, a set of parameters $\boldsymbol{\omega}$ can be also defined for the likelihood function and might include the rock physics parameters (e.g., the coordination number, critical porosity, and fluid bulk modulus) and the seismic parameters (e.g., the seismic wavelet). However, in the proposed approach, we assume that the rock physics and seismic parameters in the forward model are known.

The proposed formulation can be applied with any inversion method including analytical solutions for particular cases, such as Bayesian linearized inversion under Gaussian assumptions as in Buland and Omre (2003) and Grana (2016), and numerical sol-

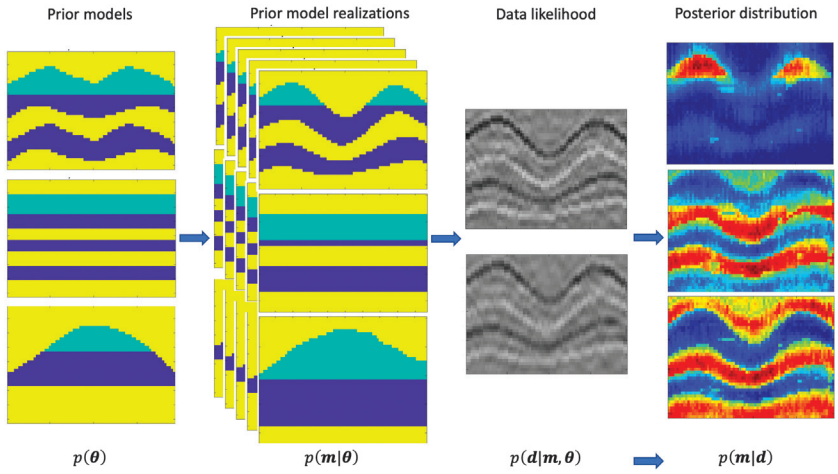

Figure 1. The workflow of the proposed methodology: A finite set of prior models is first defined, and then multiple realizations are sampled from each prior model; for each realization, the likelihood of the data is evaluated, and then the posterior distribution is assessed in a Bayesian framework.

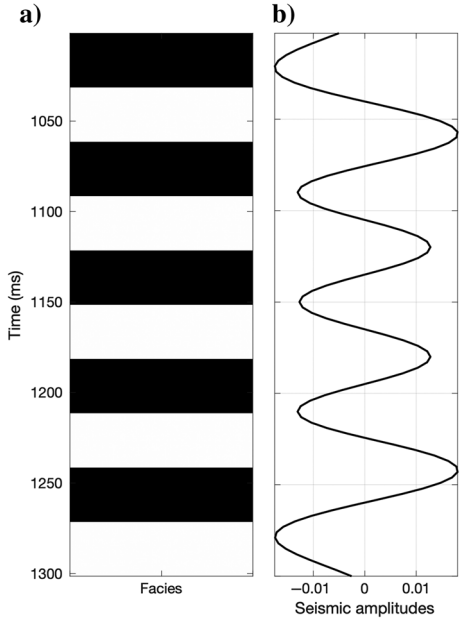

Figure 2. Example 1. Reference synthetic model at the well location: (a) the facies profile (reference model) with alternating sequence of sand (in white) and shale (in black) and (b) the synthetic seismic data (measured data).

utions, such as Monte Carlo rejection sampling and Markov-chain-Monte-Carlo (McMC) methods (Metropolis, Metropolis-Hastings, and Gibbs sampling algorithms) as in Grana et al. (2017) and de Figueiredo et al. (2019a, 2019b).

The workflow of the methodology is shown in Figure 1. First, I choose a set of prior models, then I develop the conditional probabilities $p(\boldsymbol{d}|\boldsymbol{m},\boldsymbol{\theta})$ and $p(\boldsymbol{m}|\boldsymbol{\theta})$ according to the adopted inversion approach using either numerical or analytical methods, and, finally, I compute the posterior probability using equation 6. The posterior probability of the prior models is then computed using equation 9.

APPLICATION

I validate the methodology on synthetic and real examples. Example 1 focuses on facies classification from seismic data where I adopt a stationary first-order Markov chain for the prior model of the facies. I assume that there are two facies, sand and shale, but the average thickness of the layers is uncertain. I analyze three possible geologic scenarios: sequences of moderately thick layers of sand and shale (scenario A), sequences of thick sand and thick shale layers (scenario B), and sequences of thick sand and interbedded thin shale (scenario C). Proportions of sand and shale are the same and equal to 50% in scenarios A and B; whereas in scenario C, the sand proportion is 90% and shale proportion is 10%. Example 2 is the same facies classification problem as in example 1, but in this example, I adopt training images of facies profiles for multipoint geostatistics simulations to analyze scenarios A, B, and C.

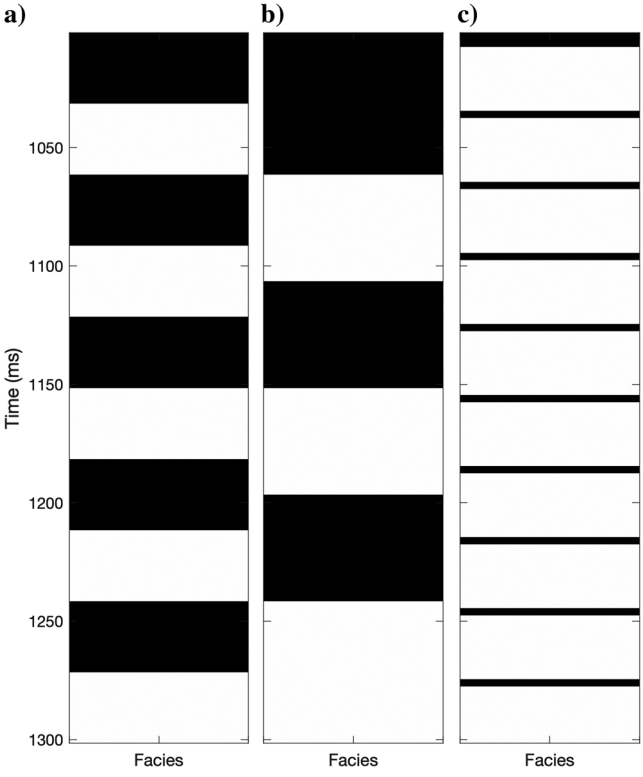

Figure 3. Example 1. Conceptual models for facies classification: (a) scenario A (reference model), (b) scenario B with thick layers, and (c) scenario C with thick sand and thin shale and predominant sand proportion. The sand facies is in white, and the shale facies is in black.

Examples 3 and 4 focus on the prediction of continuous petrophysical properties, namely porosity and clay volume, from elastic properties. Example 3 is a rock physics inversion where the number of facies is unknown, and the prior distribution of petrophysical properties is a Gaussian mixture with a variable number of components. Example 4 is a joint facies and petrophysical inversion of seismic data, in which two facies models are available, one compatible with the well log scale and one compatible with the seismic scale. Finally, example 5 is a 2D application representing a vertical section of a clastic reservoir with three lithofluid facies.

Example 1: Multiple transition matrices

In the first example, the model variable $\boldsymbol{m}$ is the facies profile, the data $\boldsymbol{d}$ are the zero-offset seismogram, and the parameters $\boldsymbol{\theta}$ are the Markov chain transition probabilities (Krumbein and Dacey, 1969). A Markov chain is a stochastic model describing a sequence of possible events (the facies occurrence, in our application) in which the probability of a given event (the facies occurrence at a given depth) depends only on the previous events (the facies occurrences at the depths above).

The true facies model is a vector of 100 samples, and it represents a sequence of five layers of shale (in black) alternated to five layers of water-saturated high-porosity sand (in white) with a constant thickness equal to 25 m. In each facies, we assume constant elastic properties. The compressional-wave velocity is 2000 m/s in shale and 2500 m/s in sand; the shear-wave velocity is 1000 m/s in shale and 1500 m/s in sand; and the density is 2.5 g/cm^3 in shale and 2.25 g/cm^3 in sand. The synthetic seismic data are obtained using Kennett's invariant imbedding method (Kennett, 1984). The Ricker wavelet has a dominant frequency of 30 Hz. The signal-to-noise ratio (S/N) is 10. The true facies model and the corresponding seismic measurements are shown in Figure 2. The three potential geologic scenarios are shown in Figure 3. Scenario A corresponds to the true model, scenario B shows a sequence of three ticker layers of shale and three ticker layers of sand, whereas scenario C shows 10 thick sand layers alternated to 10 thin shale layers (Figure 3).

The inversion is performed using a Bayesian inversion based on first-order stationary Markov chains (Krumbein and Dacey, 1969). The data error is assumed to be Gaussian with $\boldsymbol{0}$ mean and constant variances equal to 10% of the variance of the data; hence, the data likelihood given the model is Gaussian. The parameter $\boldsymbol{\theta}$ represents

Table 1. Example 1. Transition matrices of reference model and three conceptual models.

	Shale (bottom)	Sand (bottom)
Shale (top)	Reference — 0.90	Reference — 0.10
	Scenario A — 0.90	Scenario A — 0.10
	Scenario B — 0.95	Scenario B — 0.05
	Scenario C — 0.10	Scenario C — 0.90
Sand (top)	Reference — 0.10	Reference — 0.90
	Scenario A — 0.10	Scenario A — 0.90
	Scenario B — 0.05	Scenario B — 0.95
	Scenario C — 0.10	Scenario C — 0.90

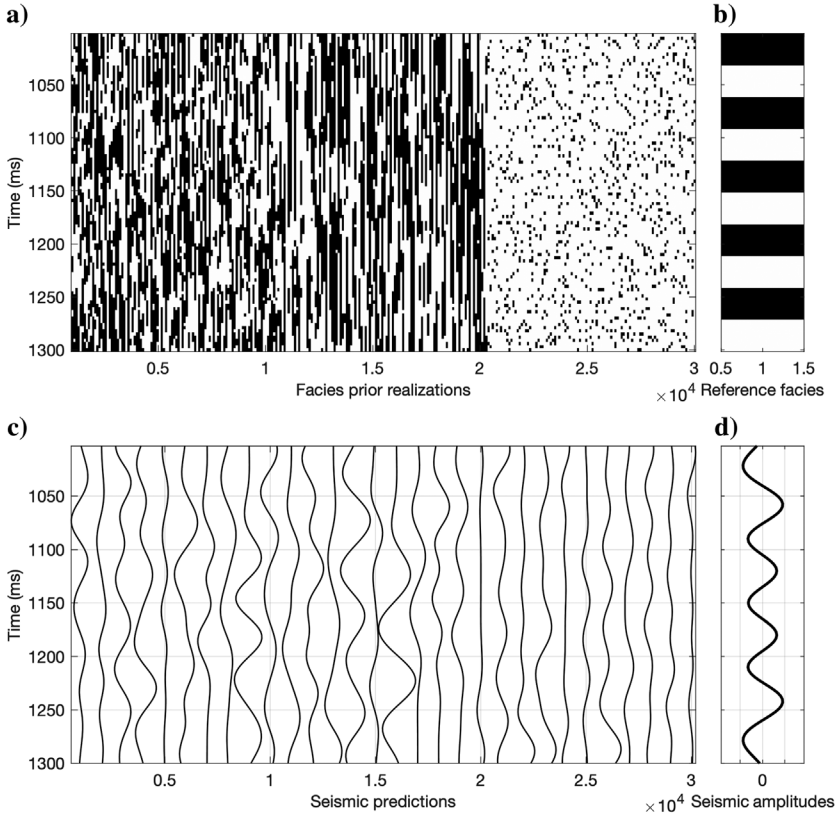

Figure 4. Example 1. Facies prior realizations and their corresponding seismic response using Markov chain simulations: (a) 300 facies prior realizations (100 for each scenario) randomly selected from an ensemble of 300,000, (b) reference facies model, (c) 30 seismic amplitude predictions of the facies prior realizations (plotted every 10), and (d) reference seismic data.

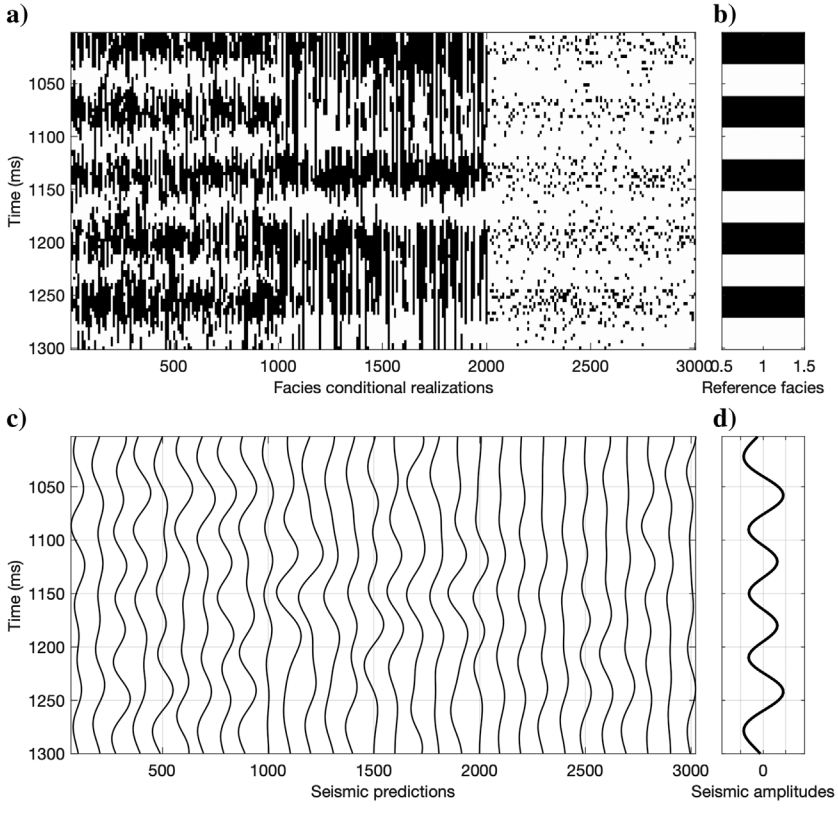

Figure 5. Example 1. Facies conditional realizations and their corresponding seismic response using Markov chain simulations: (a) 300 facies prior realizations (100 for each scenario), (b) reference facies model, (c) 30 seismic amplitude predictions of the facies conditional realizations (plotted every 10), and (d) reference seismic data.

the transition matrix T of the Markov chain model that includes the probabilities of the transition from one facies to another facies at the interfaces. The transition matrix is used to sample the facies profiles from the probability $p(\boldsymbol{m}|\boldsymbol{\theta})$: The facies value at the first depth location is sampled from the prior distribution of the facies, whereas the following facies values along the profiles are sampled from the Markov chain transition probabilities conditioned by the facies value sampled at the previous depth location. In general, the transition probability matrix is assumed to be known; however, this assumption might affect the inversion results. I propose to perform the Bayesian facies classification using three different transition matrices (Table 1) estimated from the three conceptual models in Figure 3. The transition matrix (T_1) in scenario A is the same as the one associated to the true model (0.9 probability of staying in the same facies and 0.1 probability of transitioning to the other facies); the transition matrix (T_2) in scenario B shows higher probability of staying in the same facies (0.95 probability) and lower probability to transition to the other facies (0.05); the transition matrix (T_3) in scenario C is asymmetric and shows high probabilities of staying in sand (0.9) and transitioning from shale to sand (0.9) and low probabilities of staying in shale (0.1) and transitioning from sand to shale (0.1). The transition matrices in A and B lead to the same prior proportions of 50% of sand and 50% of shale, whereas the transition matrix in C leads to shale prior proportion equal to 10% and sand prior proportion equal to 90%.

The parameters $\boldsymbol{\theta}$ include the transition probabilities of the transition matrix. I assume that the three transition matrices in scenarios A, B, and C have the same prior probability equal to 1/3 ($P(\boldsymbol{\theta} = T_i) = 1/3$ for $i = 1, 2, 3$). I then sample the facies realization, that is, a stochastic simulation of the facies profile, from the corresponding transition matrices. In Figure 4a, I sample 300,000 realizations of facies (10,000 from each transition matrix) and show 1% of the realizations (300 realizations of facies, 100 from each transition matrix). The realizations are sampled sequentially according to the transition matrix: The first facies value (at the top) is sampled from the prior distribution of facies (50% sand and 50% shale for scenarios A and B; 90% sand and 10% shale for scenario C); and then, the following values at locations k are sequentially sampled according to the probabilities $p_{i,j} = P(f_k = i|f_{k-1} = j)$ for $i, j \in \{\text{sand, shale}\}$, that is, the probabilities in the transition matrix. The seismic amplitude responses computed from the prior model are shown in Figure 4c. Because the realizations are only based on the prior transition probabilities but are not conditioned to any data, the facies profiles and their seismic responses do not match the reference model and data (Figure 4b and 4d). For comparison, I show facies conditional realizations, conditioned by seismic data, and their corresponding seismic responses in Figure 5. For each transition matrix, I show 100 conditional simulations. The prior assumptions affect the final simulations, but a coherent information in the sequence of the facies interfaces can be detected (Figure 5a).

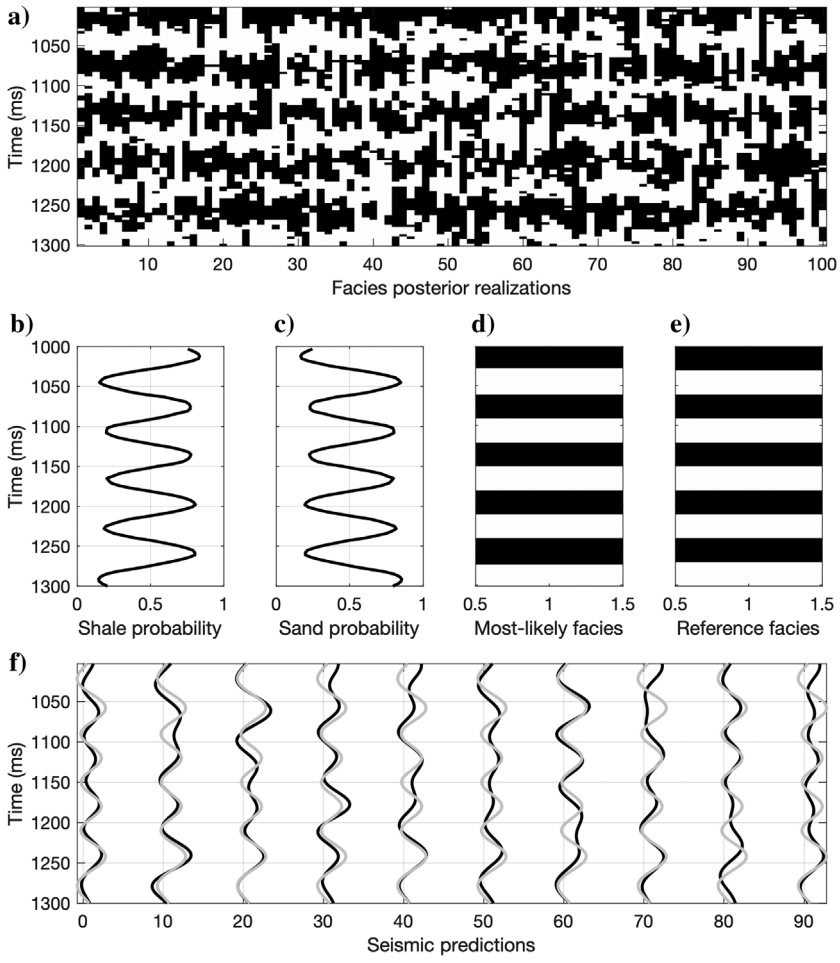

Figure 6. Example 1. Facies posterior realizations and their corresponding seismic response using Markov chain simulations: (a) 100 of 30,000 facies realizations, (b) posterior probability of shale, (c) posterior probability of sand, (d) most likely facies model, (e) reference facies model, and (f) 10 seismic amplitude predictions (plotted every 10) compared to reference seismic data (gray lines).

I first compute the probability $p(\boldsymbol{m}|\boldsymbol{d})$ of the model $\boldsymbol{m}$ given the reference data using equation 6, summing over the three possible scenarios for the parameters $\boldsymbol{\theta} = T_i$, for $i = 1, 2, 3$. The probability is computed using a Monte Carlo rejection sampling (Robert and Casella, 2013) with an acceptance rate of 10% (30,000 realizations). The Monte Carlo rejection sampling generates samples from the posterior distribution by using a uniform proposal distribution and accepting or rejecting samples according to the likelihood function. The posterior probability is shown in Figure 6; the probability of sand and shale, as well as the most likely facies model, match the facies reference model. Figure 6a shows 100 posterior realizations, to illustrate the variability of the solutions.

I then compute the probability $p(\boldsymbol{\theta}|\boldsymbol{d})$ of the parameters $\boldsymbol{\theta}$ given the reference data using equation 9. The three transition matrices are assumed to be equiprobable; therefore, $P(\boldsymbol{\theta}) = 1/3$ for every $\boldsymbol{\theta}$, and the probability $P(\boldsymbol{d})$ is a normalizing constant. Hence, the probability $p(\boldsymbol{\theta}|\boldsymbol{d})$ reduces to the computation of the sum in equation 9, where the two probabilities are obtained from the Monte Carlo sampling. The conditional probability $p(\boldsymbol{\theta}|\boldsymbol{d})$ becomes $P(\boldsymbol{\theta} = T_1|\boldsymbol{d}) = 0.83$, $P(\boldsymbol{\theta} = T_2|\boldsymbol{d}) = 0.06$, and $P(\boldsymbol{\theta} = T_3|\boldsymbol{d}) = 0.11$, and this shows that the most likely set of parameters is represented by the transition matrix T_1 of scenario A, which is indeed the transition matrix of the true model. If I decrease the S/N) of the data to five and repeat the inversion, the results are still consistent: $P(\boldsymbol{\theta} = T_1|\boldsymbol{d}) = 0.72$, $P(\boldsymbol{\theta} = T_2|\boldsymbol{d}) = 0.14$, and $P(\boldsymbol{\theta} = T_3|\boldsymbol{d}) = 0.14$. However, if I decrease $S/N = 2$, the probabilities tend to regress toward the prior, $P(\boldsymbol{\theta} = T_1|\boldsymbol{d}) = 0.59$; $P(\boldsymbol{\theta} = T_2|\boldsymbol{d}) = 0.22$; and $P(\boldsymbol{\theta} = T_3|\boldsymbol{d}) = 0.19$; and with $S/N = 1.25$, the results become $P(\boldsymbol{\theta} = T_1|\boldsymbol{d}) = 0.42$, $P(\boldsymbol{\theta} = T_2|\boldsymbol{d}) = 0.29$, and $P(\boldsymbol{\theta} = T_3|\boldsymbol{d}) = 0.28$.

Example 2: Multiple training images

In the second example, I repeat the same exercise using multipoint geostatistics simulations using training images (Mariethoz and Caers, 2014). The aim of multipoint geostatistics is to generate a realization of subsurface properties with complex spatial correlations and structures (e.g., connectivity and stacking patterns). In multipoint geostatistics, the spatial correlation of the model variables and the conditional probabilities for the simulation are inferred from a training image that represents a conceptual geologic model (Mariethoz and Caers, 2014). I adopt the direct sampling simulation (DSS) method (Mariethoz et al., 2010), but any other algorithm, such as single-normal equation simulation (SNESIM) or simulation of patterns (SIMPAT), could be used (Mariethoz and Caers, 2014). In the context of facies simulations, DSS sequentially simulates samples along the facies profile according to a random path of the depth locations and uses the previously simulated samples (at different depth locations) as conditioning data. Differently from Markov-chain models (example 1), where only the sample above is used, in DSS the entire set of previously simulated samples is used. The new sample is generated according to the similarity of the simulated samples with the patterns observed in the training image (Mariethoz et al., 2010).

The inversion problem is the same as in example 1, with the same likelihood function, but the prior models are the training images. I assume three possible (equiprobable) training images represented by the conceptual models in Figure 3. The prior probability is uniform, $P(\boldsymbol{\theta} = \mathrm{TI}_i) = 1/3$ for $i = 1, 2, 3$. The prior realizations are shown in Figure 7. Similar to the previous example, the posterior probability $p(\boldsymbol{m}|\boldsymbol{d})$ of the model $\boldsymbol{m}$ given the data is computed using a Monte Carlo rejection sampling method. The posterior realiza-

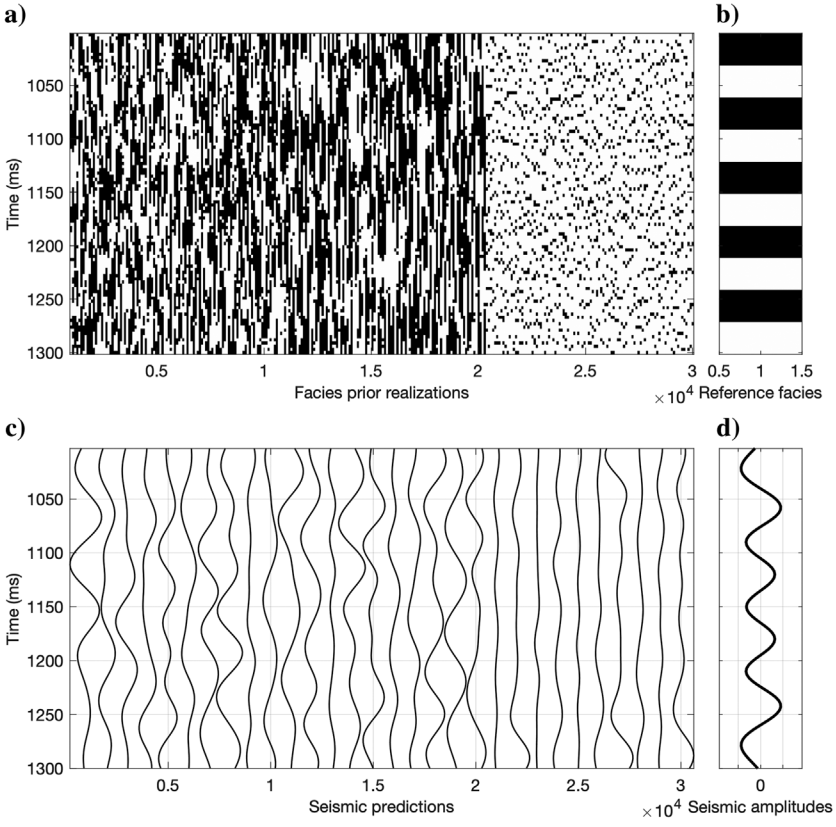

Figure 7. Example 2. Facies prior realizations and their corresponding seismic response using multipoint geostatistics simulations: (a) 300 facies prior realizations (100 for each scenario) randomly selected from an ensemble of 300,000, (b) reference facies model, (c) 30 seismic amplitude predictions of the facies prior realizations (plotted every 10), and (d) reference seismic data.

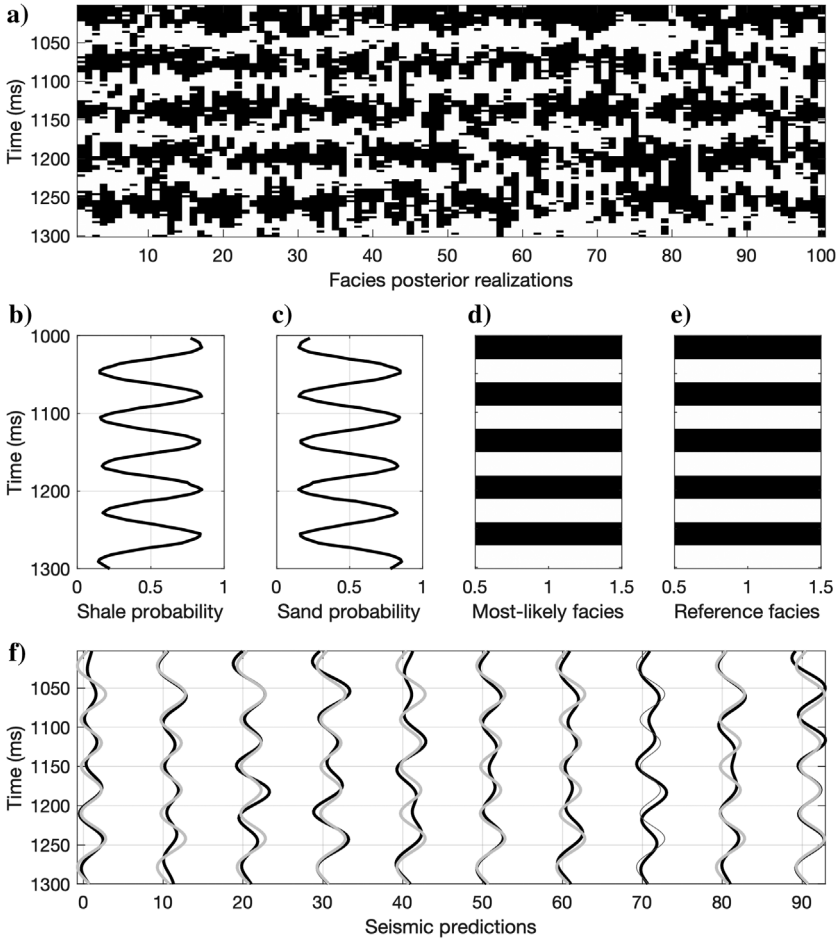

Figure 8. Example 2. Facies posterior realizations and their corresponding seismic response using multipoint geostatistics simulations: (a) 100 of 30,000 facies realizations, (b) posterior probability of shale, (c) posterior probability of sand, (d) most likely facies model, (e) reference facies model, and (f) 10 seismic amplitude predictions (plotted every 10) compared to reference seismic data (the gray lines).

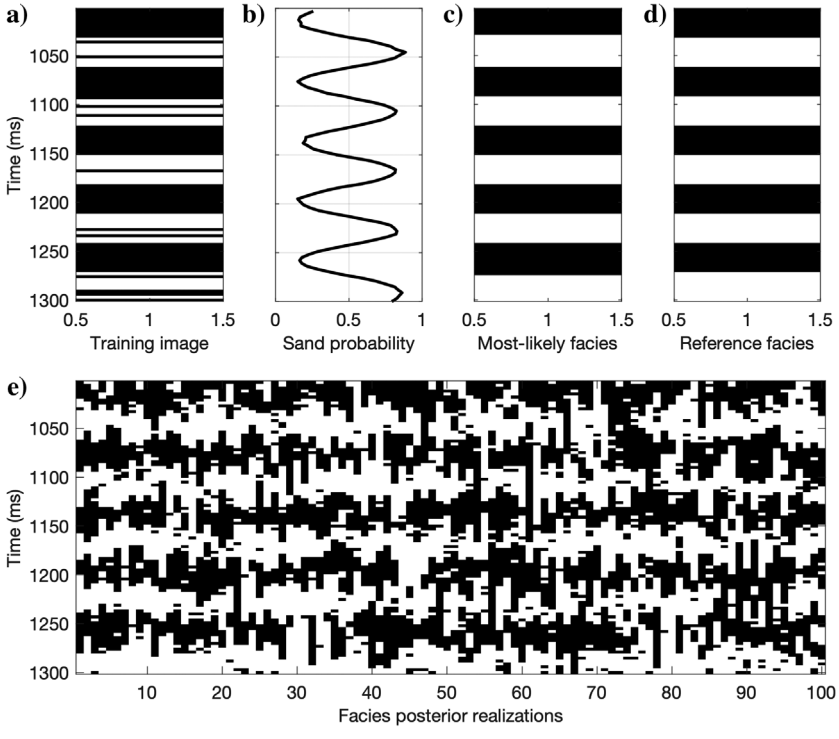

Figure 9. Example 2. Facies posterior realizations with additional training image: (a) additional training image with interbedded shale in sand layers, (b) posterior probability of sand, (c) most likely facies model, (d) reference facies model, and (e) 100 of 30,000 facies realizations.

tions are shown in Figure 8. Despite the different simulation methods, that is, multipoint geostatistics based on training images rather than sequential simulations using Markov-chain transition matrices, the results are very consistent with those in Figure 6.

I then compute the probability $p(\boldsymbol{\theta}|\boldsymbol{d})$ of the training images TI_i for $i = 1, 2, 3$ given the observed seismic data. According to the computed conditional probability $p(\boldsymbol{\theta}|\boldsymbol{d})$, $P(\boldsymbol{\theta} = \mathrm{TI}_1|\boldsymbol{d}) = 0.74$; $P(\boldsymbol{\theta} = \mathrm{TI}_2|\boldsymbol{d}) = 0.22$; and $P(\boldsymbol{\theta} = \mathrm{TI}_3|\boldsymbol{d}) = 0.04$, the most likely set of parameters is represented by the training image TI_1 of scenario A, that corresponds to the true conceptual model.

I then repeat the same numerical experiment, but with an additional training image (Figure 9a) that shows shale layers alternated to sand layers with interbedded thin shale. This additional training image is potentially compatible with the measured data since the interbedded shale layers within sand layers are below seismic resolution. The prior distribution of the training images is uniform; hence, the prior probability of each training image is $P(\boldsymbol{\theta} = \mathrm{TI}_i) = 0.25$, for $i = 1, \ldots, 4$. The results of the inversion are shown in Figure 9. The most likely model is similar to the one obtained in Figure 8 (using only three training images), but the posterior realizations show some interbedded shale layers. These layers come from the prior model and are not rejected by the data likelihood. Indeed, the computed conditional probability of the prior parameters show high values for TI_1 (i.e., the reference model) and TI_4 (i.e., the additional training image with interbedded shale layers), $P(\boldsymbol{\theta} = \mathrm{TI}_1) = 0.64$; $P(\boldsymbol{\theta} = \mathrm{TI}_2) = 0.01$; $P(\boldsymbol{\theta} = \mathrm{TI}_3) = 0.04$; and $P(\boldsymbol{\theta} = \mathrm{TI}_4) = 0.31$.

Example 3: Multimodal continuous distributions with a different number of modes

The third example is an inverse problem with continuous properties. The model variable $\boldsymbol{m}$ represents the porosity and the volume of clay, and the data $\boldsymbol{d}$ represent P- and S-impedance. The parameter $\boldsymbol{\theta}$ represents the number of modes in the multimodal distribution of petrophysical properties. The prior number of modes is assumed to be finite and relatively small, given the limited range of the petrophysical values. I assume that the prior distribution of petrophysical properties is a Gaussian mixture model, and I apply a Bayesian rock-physics inversion method to predict the point-wise posterior probability of the model given the data as in Grana and Della Rossa (2010). For a given value of the parameter $\boldsymbol{\theta}$ (i.e., the number of modes of the multimodal distribution), the solution of the inverse problem is analytically tractable under the Gaussian mixture assumption (Grana and Della Rossa, 2010).

The method is applied to a set of measurements extracted from a well log data set in a clastic reservoir. The well-log samples are measured in a sequence of sand and shale. The measured elastic data are shown in Figure 10. The prior distributions of petrophysical properties with a variable number of modes are shown in Figure 11. I assume that the number of modes (i.e., the number of components of the Gaussian mixture model) is an integer between one and three.

I then compute the posterior distribution $p(\boldsymbol{m}|\boldsymbol{d})$ of petrophysical properties conditioned by impedances using a Bayesian Gaussian mixture inversion assuming a linearized rock physics model in each component as in Grana et al. (2017). Differently from the previous two examples, the inversion does not include a spatial correlation

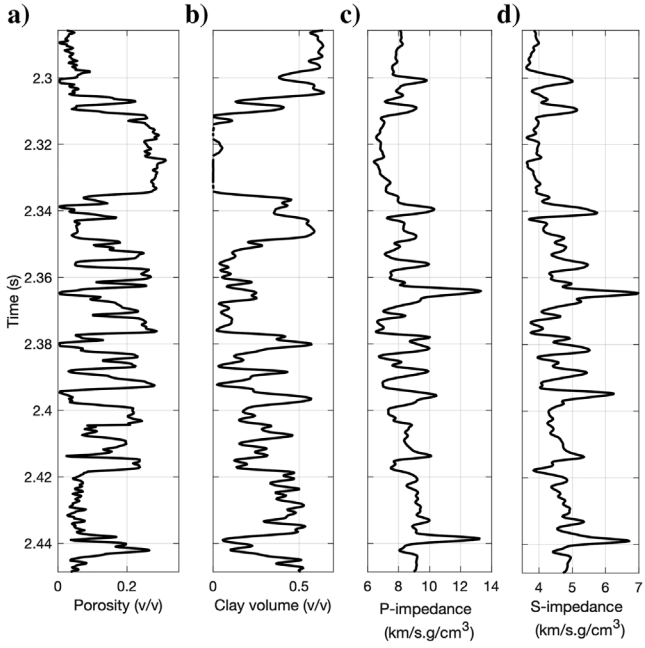

Figure 10. Example 3. Reference well log data: (a) porosity, (b) volume of clay, (c) P-impedance, and (d) S-impedance.

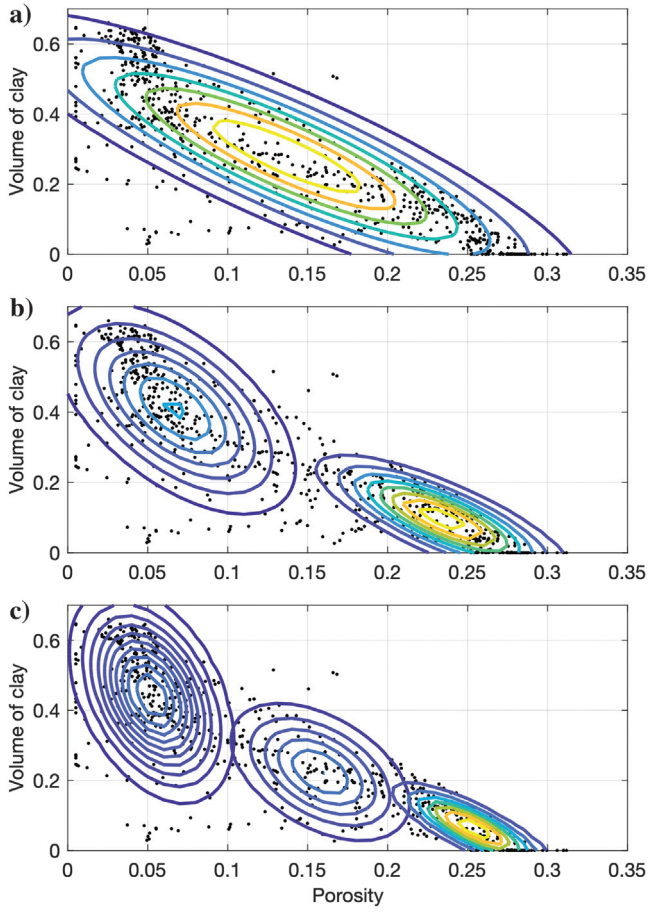

Figure 11. Example 3. Prior distribution of petrophysical properties with three different modes: from (a) to (c) the number of modes increases from one to three. The black dots represent the data, and the colored lines represent the probability contours of the Gaussian components.

model and the solution can be analytically computed at each point for each number of modes. The posterior distribution is then obtained by summing over all the possible prior models as in equation 6. The results are shown in Figure 12a and 12b and show a good agreement with the reference petrophysical curves. The distribution $p(\boldsymbol{\theta}|\boldsymbol{d})$ is also computed. The results are shown in Figure 12c. In general, the multimodal models (with two or three modes) have higher likelihood than the unimodal model. However, at many points, the models with two and three modes have similar likelihood (between 0.35 and 0.40). Therefore, both models with two and three modes could be applied in this inversion.

Example 4: Mixed discrete-continuous distribution

In this example, the data set is the set of well logs shown in Figure 10 and corresponding seismograms (Figure 13). The model variables $\boldsymbol{m}$ include facies in addition to porosity and clay volume. First, we apply the inversion to sonic logs, and then to near and far seismograms. The parameters $\boldsymbol{\theta}$ are the number of modes and the transition probabilities of the Markov chain. I assume that only two cases are possible eight facies with the transition matrix shown in Table 2 (model A) and three facies with the transition matrix shown in Table 3 (model B). Model 8 has been defined based on depositional models using core analysis; model B is a simplified model based on the facies discriminability using elastic logs. The facies profiles for both scenarios are shown in Figure 13c and 13d. In model A, the eight facies include marine silty-shale, prodelta, flood plain, mouth bar, distributary channel, crevasse splay, tidal deltaic lobes, and tight formations. In model B, the three facies represent sand, silt, and shale.

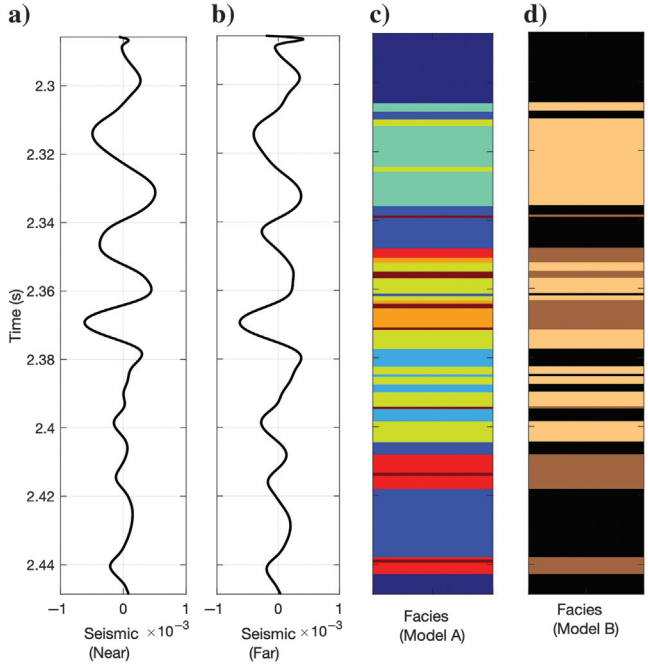

Figure 13. Example 4: Seismic data and facies classification included in the data set in Figure 10: (a) seismogram (near angle, 8°), (b) seismogram (far angle, 25°), (c) facies profile (eight facies model), and (d) facies profile (three facies model). In the facies profiles, the colors represent the marine silty-shale in dark blue, prodelta in blue, flood plain in light blue, mouth bar in green, distributary channel in yellow, crevasse splay in orange, tidal deltaic lobes in red, and tight formations in brown (model A); sand in yellow, silt in brown, and shale in black (model B).

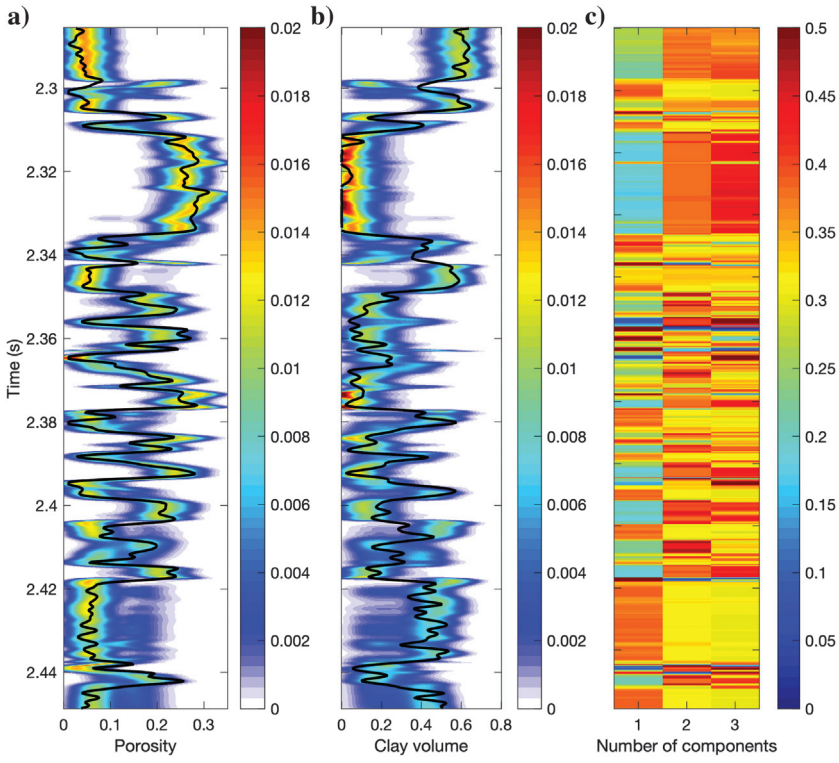

Figure 12. Example 3. Posterior distribution of the Bayesian inversion method: (a) posterior distribution of porosity, (b) posterior distribution of volume of clay, and (c) posterior distribution of the number of components of the Gaussian mixture. The color represents the posterior probability at each point.

For each of the two models, I apply the inversion methodology presented in Grana and Della Rossa (2010) in a multivariate setting. The prior transition matrices are shown in Tables 2 and 3. Sets of multiple prior (unconditional) realizations of the facies profiles are shown in Figure 14 for both scenarios, for three and eight facies. The prior distributions of the continuous petrophysical properties, the porosity and the volume of clay, are shown in Figure 14. Because of the large prior variance of the petrophysical properties in each facies, many components overlap and the resulting distributions are bimodal (low-porosity clay and high-porosity sand). The distributions of petrophysical properties are assumed to be the same along the vertical profile.

I first apply the inversion to well log data, P-impedance and S-impedance, for the prediction of facies, the porosity and the volume of clay. The results are shown in Figure 15. The model with eight facies has a higher posterior probability. Indeed, the probability $p(\boldsymbol{\theta}|\boldsymbol{d})$ for model A is 0.78 and the probability $p(\boldsymbol{\theta}|\boldsymbol{d})$ for model B is 0.22. The uncertainty in the posterior probability of the petrophysical properties, the porosity and the volume of clay, is relatively small, and the predictions are accurate. I then apply the inversion to the seismic trace, near and far offsets (corresponding to 8° and 25° angles). The results (Figure 16) are clearly affected by the low resolution of the data. In this case, the model with three facies has a higher posterior probability: The probability $p(\boldsymbol{\theta}|\boldsymbol{d})$ for model A is 0.47, and the probability $p(\boldsymbol{\theta}|\boldsymbol{d})$ for model B is 0.53. The data are compatible with models A and B probably because most of the thin layers in model A are below seismic resolution and their elastic properties are close to the average. The conditional means for porosity and volume of clay tend to converge to the modes of the model with less components. The most likely facies model is less accurate than in the previous case. However, this could be due to the nonstationarity of the true model, which is hard to reproduce with stationary Markov chains or training images (Doyen, 2007).

Example 5: 2D application

I finally apply the proposed methodology to a facies classification problem of a 2D seismic section. The reference model is presented in de Figueiredo et al. (2019b) and is shown in Figure 17. The model includes two potential sand reservoir layers surrounded by shale layers. The top reservoir is filled by oil and water, whereas the bottom reservoir is filled by water only. The data set includes four angle stacks corresponding to 12.5°, 25°, 37.5°, and 50°, with an average frequency of 37, 32, 29.5, and 27 Hz, respectively. The S/N is 10. The seismic data are shown in Figure 18. Three different conceptual models were build using object modeling (Caers, 2011) to test the methodology: a model with flat layers (model C_1, Figure 17b), an anticline model (model C_2, Figure 17c), and a structural model interpreted from the seismic data (model C_3, Figure 17d).

The inversion was performed using a Monte Carlo approach. I first generate a set of 100 facies realizations for each prior model in Figure 17, using object modeling. Due to the dimension of the data set, I use multidimensional scaling (Caers, 2011; Azevedo et al., 2013) to evaluate the conditional probabilities $p(\boldsymbol{d}|\boldsymbol{m},\boldsymbol{\theta})$ and $p(\boldsymbol{m}|\boldsymbol{\theta})$ in a lower dimensional space. The posterior distribution is computed using equation 6. The posterior probabilities of the three facies are shown in Figure 19 with the most likely model. In this example, the results show that the prior models C_1 and C_2 are not compatible with the data. Indeed, the posterior probabilities of the three conceptual models, computed using equation 9, are $P(\boldsymbol{\theta} = C_1) = 0.05$, $P(\boldsymbol{\theta} = C_2) = 0.01$, and $P(\boldsymbol{\theta} = C_3) = 0.94$.

DISCUSSION

The presented workflow is very general and can be applied in combination with any Bayesian inverse method. Indeed, it can be applied with analytical methods for Bayesian inversion or classification as well as the Monte Carlo and McMC algorithms. In general, the implementation of the method is simple when the number of possible values of the prior parameters is limited because the posterior distribution can be obtained as a sum over all the possible prior parameters. Examples of applications include facies classification with different training images or transition matrices and petrophysical inversion with Gaussian mixture with different numbers of components (i.e., modes). For continuous parameters, the solution of the integral might not be analytically tractable, except for

Table 3. Example 4. Transition matrix for three facies model.

	Shale	Silt	Sand
Shale	0.97	0.01	0.02
Silt	0.03	0.95	0.02
Sand	0.03	0.01	0.96

Table 2. Example 4. Transition matrix for eight facies model.

	Marine s. shale	Prodelta	Flood plain	Mouth bar	Dist. channel	Crevasse splay	Tidal d. lobes	Tight
Marine s. shale	0.99	0.00	0.00	0.01	0.00	0.00	0.01	0.00
Prodelta	0.00	0.96	0.00	0.00	0.01	0.00	0.02	0.01
Flood plain	0.00	0.00	0.92	0.00	0.08	0.00	0.00	0.00
Mouth bar	0.00	0.01	0.00	0.97	0.01	0.00	0.00	0.00
Dist. Channel	0.00	0.01	0.02	0.02	0.93	0.01	0.00	0.01
Crevasse splay	0.00	0.00	0.00	0.00	0.03	0.92	0.00	0.05
Tidal d. lobes	0.01	0.01	0.00	0.00	0.00	0.02	0.93	0.03
Tight	0.00	0.03	0.03	0.00	0.06	0.04	0.06	0.78

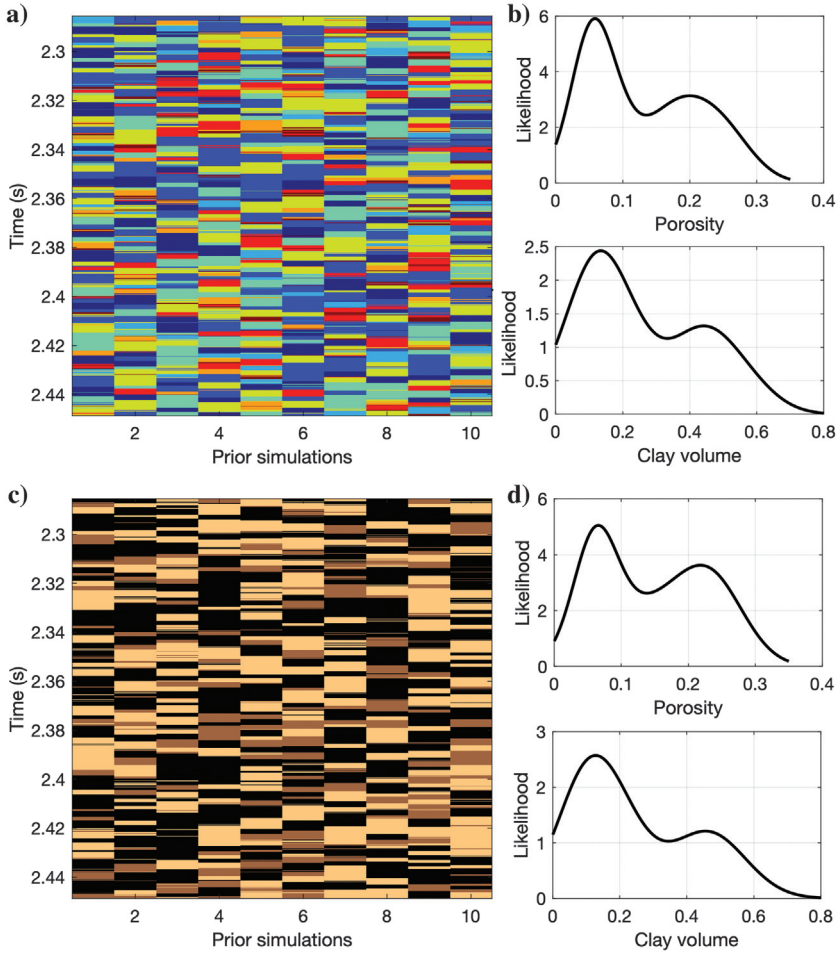

Figure 14. Example 4. Prior geostatistical simulations of facies and prior distributions of petrophysical properties: (a) prior realizations using eight facies and the corresponding transition matrix, (b) prior distributions of porosity and volume of clay based on 8C Gaussian mixture model, (c) prior realizations using three facies and the corresponding transition matrix, and (d) prior distributions of porosity and volume of clay based on 3C Gaussian mixture model.

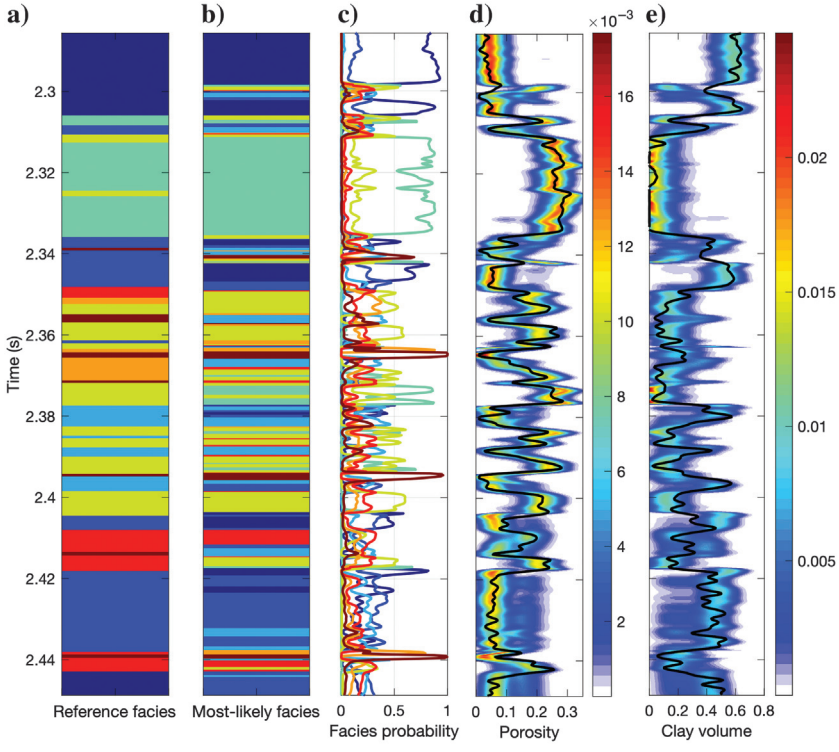

Figure 15. Example 4. Posterior distributions conditioned by well log data: (a) reference facies (model A), (b) most likely facies model, (c) posterior distribution of facies, (d) posterior distribution of porosity, and (e) posterior distribution of volume of clay. The black lines in (d and e) represent the actual well log.

Gaussian linear likelihood and Gaussian prior models; therefore, the integral should be approximated by discretizing the parameter space. All of the examples assume a limited number of prior models (between two and four), but the approach could be extended to a larger number of prior models.

The computational cost of the methodology mostly depends on the algorithm used for the Bayesian inversion method and the choice of the forward model used for the likelihood evaluation. The inversion with multiple priors can run in parallel because each inversion is independent from the others. The approach can be applied using different forward operators: convolutional models of Zoeppritz equations, Kennett's invariant imbedding method, the Born weak scattering approximation, as well as different rock-physics relations. Theoretically, the formulation could be extended to the full-waveform inversion but it would require advanced computational methods to make the computational cost feasible, and McMC

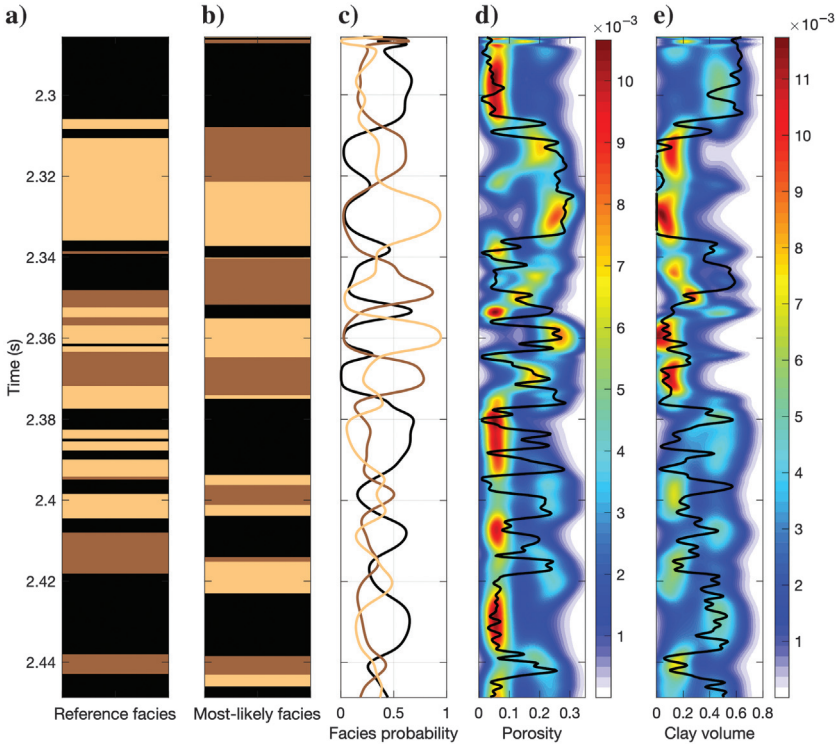

Figure 16. Example 4. Posterior distributions conditioned by seismic data: (a) reference facies (model B), (b) most likely facies model, (c) posterior distribution of facies, (d) posterior distribution of porosity, and (e) posterior distribution of volume of clay. The black lines in (d and e) represent the actual well log.

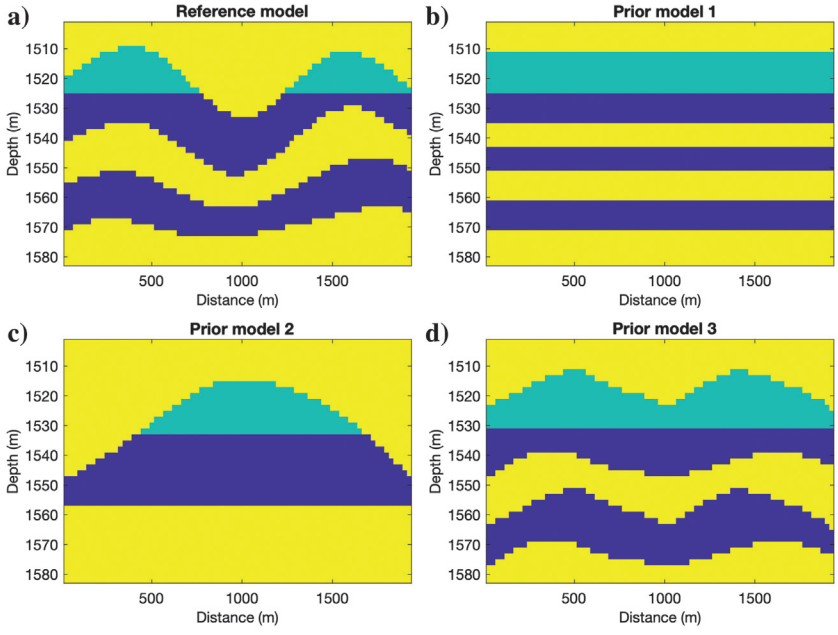

Figure 17. Example 5. Two-dimensional synthetic model: (a) reference facies model, (b) prior model 1 with flat layers, (c) prior model 2 with an anticline structure, and (d) prior model 3 with a geologic structure interpreted from seismic data. The shale is in yellow, water sand is in blue, and oil sand is in green.

methods should be replaced with faster and highly parallelizable stochastic algorithms, such as gradual deformation and ensemble-based methods. The proposed approach could be extended to the parameters of the forward operator, such as the rock physics parameters and the seismic wavelet. Advanced geostatistical methods based on nonstationary assumptions (Mariethoz and Caers, 2014) could also be applied.

In real data applications, several parameters and assumptions of the model, such as the wavelet, the S/N, the rock-physics parameters, and the number of facies, should be included in the study before applying the proposed inversion workflow because these elements could affect the uncertainty in the posterior distributions of the model variables. In the proposed examples, the wavelet is assumed to be known and accurate; therefore, there is no uncertainty associated with the wavelet. However, in practical studies, the wavelet is statistically extracted from the data and such estimation could be uncertain. Similarly, the measurement errors are often assumed to be Gaussian and uncorrelated and the covariance matrix of the errors in the measurements is generally assumed to be diagonal with the same variance for all the measurements. However, seismic processing could introduce correlated errors in the data, which can affect the assessment of the posterior uncertainty. In this case, the covariance should be a full matrix built using a correlation function for the data error.

Geostatistical methods allow the generation of multiple realizations of the model properties to capture the model uncertainty; however, in many practical applications only a limited number of models are used for model forecasting and decision making. The uncertainty quantification is generally summarized through a set of statistical estimators, such as P10, P50, and P90 of the properties of interest (e.g., the total oil in place or the net pay). Posterior probabilities can be embedded in decision trees and the uncertainty quantification in the predicted results is valuable in decision-making processes (Caers, 2011).

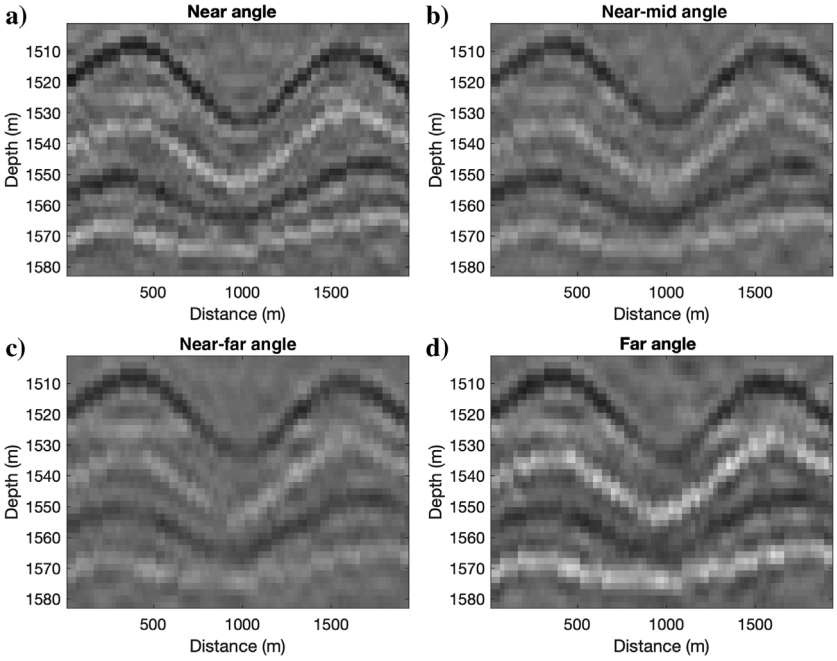

Figure 18. Example 5. Partial-stacked seismic data: (a) angle stack 12.5°, (b) angle stack 25°, (c) angle stack 37.5°, and (d) angle stack 50°.

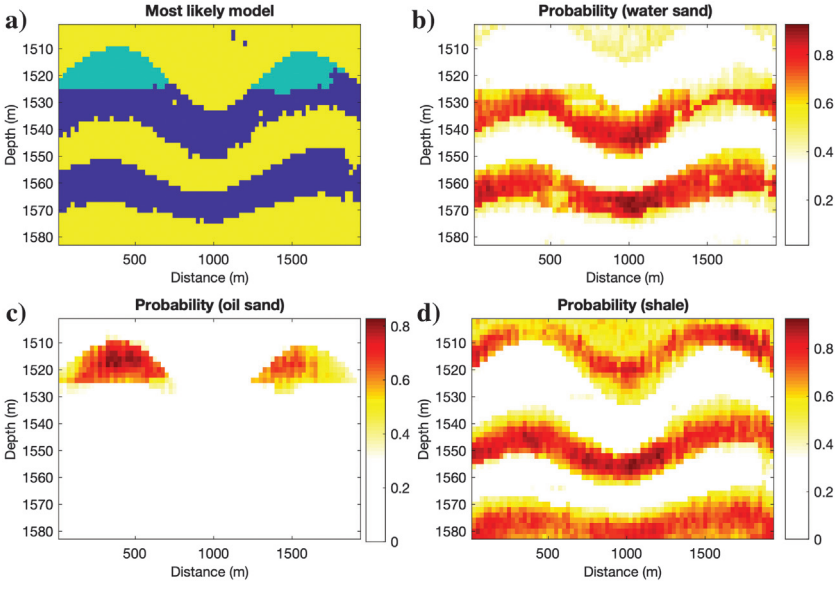

Figure 19. Example 5. Bayesian inversion results (a) most likely facies model, (b) posterior probability of water-sand facies, (c) posterior probability of oil-sand facies, and (d) posterior probability of shale facies. The colors in plot (a) represent the facies (shale in yellow, water sand in blue, and oil sand in green). The colors in plots (b-d) represent the posterior facies probability.

CONCLUSION

I presented a mathematical formulation for a general Bayesian inversion problem with multiple prior models. The method can be applied to discrete and continuous random variables for inversion and classification problems. The formulation provides the posterior density function of the model parameters conditioned by the observed data, as well as the posterior distribution of the model parameters given the data. The probability of the model given the data is the solution of the inverse problem in a Bayesian setting, and it is the obtained by summing all of the likelihood functions weighted by the prior probabilities. The probability of the model parameters represents how compatible the prior model is with the observed data. Therefore, the proposed method can be used to discard prior models that might be geologically acceptable but that are inconsistent with the data. The formulation with multiple prior models leads to a better

representation of the uncertainty in the model predictions due to the uncertainty in the model parameters.

ACKNOWLEDGMENTS

The author acknowledges the School of Energy Resources of the University of Wyoming for supporting this research.

DATA AND MATERIALS AVAILABILITY

Data associated with this research are available and can be obtained by contacting the corresponding author.

REFERENCES

Aki, K., and P. G. Richards, 1980, Quantitative seismology: Freeman.
Anderson, T., 1984, An introduction to multivariate statistical analysis: Wiley, Wiley series in probability and mathematical statistics: Probability and mathematical statistics.
Azevedo, L., R. Nunes, P. Correia, A. Soares, L. Guerreiro, and G. S. Neto, 2013, Multidimensional scaling for the evaluation of a geostatistical seismic elastic inversion methodology: Geophysics, **79**, no. 5, M1–M10, doi: 10.1190/geo2013-0037.1.
Bortoli, L. J., F. A. Alabert, A. Haas, and A. G. Journel, 1993, Constraining stochastic images to seismic data: Proceedings of the 4th International Geostatistical Congress, 325–337.
Bosch, M., T. Mukerji, and E. F. González, 2010, Seismic inversion for reservoir properties combining statistical rock physics and geostatistics: A review: Geophysics, **75**, no. 5, 75A165–75A176, doi: 10.1190/1.3478209.
Buland, A., and H. Omre, 2003, Bayesian linearized AVO inversion: Geophysics, **68**, 185–198, doi: 10.1190/1.1543206.
Caers, J., 2011, Modeling uncertainty in the earth sciences: John Wiley & Sons.
Chen, J., G. M. Hoversten, D. Vasco, Y. Rubin, and Z. Hou, 2007, A Bayesian model for gas saturation estimation using marine seismic AVA and CSEM data: Geophysics, **72**, no. 2, WA85–WA95, doi: 10.1190/1.2435082.
Connolly, P. A., and M. J. Hughes, 2016, Stochastic inversion by matching to large numbers of pseudo-wells: Geophysics, **81**, no. 2, M7–M22, doi: 10.1190/geo2015-0348.1.
Contreras, A., C. Torres-Verdin, K. Kvien, T. Fasnacht, and W. Chesters, 2005, AVA stochastic inversion of pre-stack seismic data and well logs for 3D reservoir modeling: 67th Annual International Conference and Exhibition, EAGE, Extended Abstract.
de Figueiredo, L. P., D. Grana, M. Roisenberg, and B. B. Rodrigues, 2019a, Gaussian mixture Markov chain Monte Carlo method for linear seismic inversion: Geophysics, **84**, no. 3, R463–R476, doi: 10.1190/geo2018-0529.1.
de Figueiredo, L. P., D. Grana, M. Roisenberg, and B. B. Rodrigues, 2019b, Multimodal Markov chain Monte Carlo method for nonlinear petrophysical seismic inversion: Geophysics, **84**, no. 5, M1–M13, doi: 10.1190/geo2018-0839.1.
Doyen, P., 2007, Seismic reservoir characterization: EAGE.
Doyen, P. M., 1988, Porosity from seismic data: A geostatistical approach: Geophysics, **53**, 1263–1275, doi: 10.1190/1.1442404.
Eidsvik, J., P. Avseth, H. Omre, T. Mukerji, and G. Mavko, 2004, Stochastic reservoir characterization using prestack seismic data: Geophysics, **69**, 978–993, doi: 10.1190/1.1778241.
Grana, D., 2016, Bayesian linearized rock-physics inversion: Geophysics, **81**, no. 6, D625–D641, doi: 10.1190/geo2016-0161.1.
Grana, D., and E. Della Rossa, 2010, Probabilistic petrophysical-properties estimation integrating statistical rock physics with seismic inversion: Geophysics, **75**, no. 3, O21–O37, doi: 10.1190/1.3386676.
Grana, D., T. Fjeldstad, and H. Omre, 2017, Bayesian Gaussian mixture linear inversion for geophysical inverse problems: Mathematical Geosciences, **49**, 1–23, doi: 10.1007/s11004-016-9671-9.
Gunning, J., and M. Glinsky, 2007, Detection of reservoir quality using Bayesian seismic inversion: Geophysics, **72**, no. 3, R37–R49, doi: 10.1190/1.2713043.
Haas, A., and O. Dubrule, 1994, Geostatistical inversion — A sequential method of stochastic reservoir modeling constrained by seismic data: First Break, **12**, 561–569, doi: 10.3997/1365-2397.1994034.
Kemper, M., and J. Gunning, 2014, Joint impedance and facies inversion–Seismic inversion redefined: First Break, **32**, 89–95.
Kennett, B. L. N., 1984, Guided wave propagation in laterally varying media — 1: Theoretical development: Geophysical Journal International, **79**, 235–255, doi: 10.1111/j.1365-246X.1984.tb02853.x.
Krumbein, W. C., and M. F. Dacey, 1969, Markov chains and embedded Markov chains in geology: Mathematical Geology, **1**, 79–96, doi: 10.1007/BF02047072.
Mariethoz, G., and J. Caers, 2014, Multiple-point geostatistics: Stochastic modeling with training images: John Wiley & Sons.
Mariethoz, G., P. Renard, and J. Straubhaar, 2010, The direct sampling method to perform multiple-point geostatistical simulations: Water Recourses Research, **46**, W11536, doi: 10.1029/2008WR007621.
Mavko, G., T. Mukerji, and J. Dvorkin, 2009, The rock physics handbook: Cambridge University Press.
Miller, C. R., and P. S. Routh, 2007, Resolution analysis of geophysical images: Comparison between point spread function and region of data influence measures: Geophysical Prospecting, **55**, 835–852, doi: 10.1111/j.1365-2478.2007.00640.x.
Mosegaard, K., 1998, Resolution analysis of general inverse problems through inverse Monte Carlo sampling: Inverse Problems, **14**, 405–426, doi: 10.1088/0266-5611/14/3/004.
Mosegaard, K., and A. Tarantola, 1995, Monte Carlo sampling of solutions to inverse problems: Journal of Geophysical Research, **100**, 12431–12447, doi: 10.1029/94JB03097.
Mukerji, T., A. Jørstad, P. Avseth, G. Mavko, and J. R. Granli, 2001, Mapping lithofacies and pore-fluid probabilities in a North Sea reservoir: Seismic inversions and statistical rock physics: Geophysics, **66**, 988–1001, doi: 10.1190/1.1487078.
Mukerji, T., G. Mavko, and P. Rio, 1997, Scales of reservoir heterogeneities and impact of seismic resolution on geostatistical integration: Mathematical Geology, **29**, 933–950, doi: 10.1023/A:1022307807851.
Oldenburg, D.W., and Y. Li, 1999, Estimating depth of investigation in dc resistivity and IP surveys: Geophysics, **64**, 403–416, doi: 10.1190/1.1444545.
Papoulis, A., 1984, Probability, random variables and stochastic processes: McGraw-Hill.
Park, H., C. Scheidt, D. Fenwick, A. Boucher, and J. Caers, 2013, History matching and uncertainty quantification of facies models with multiple geological interpretations: Computers and Geosciences, **17**, 609–621, doi: 10.1007/s10596-013-9343-5.
Rimstad, K., P. Avseth, and H. Omre, 2012, Hierarchical Bayesian lithology/fluid prediction: A North Sea case study: Geophysics **77**, no. 2, B69–B85, doi: 10.1190/geo2011-0202.1.
Robert, C., and G. Casella, 2013, Monte Carlo statistical methods: Springer Science & Business Media.
Scales, J. A., and L. Tenorio, 2001, Prior information and uncertainty in inverse problems: Geophysics, **66**, 389–397, doi: 10.1190/1.1444930.
Scheidt, C., C. Jeong, T. Mukerji, and J. Caers, 2015, Probabilistic falsification of prior geologic uncertainty with seismic amplitude data: Application to a turbidite reservoir case: Geophysics, **80**, no. 5, M89–M100, doi: 10.1190/geo2015-0084.1.
Scheidt, C., L. Li, and J. Caers, 2018, Bayesian evidential learning: In quantifying uncertainty in subsurface systems: American Geophysical Union, Geophysical Monograph Series.
Sen, M., and P. Stoffa, 1996, Bayesian inference, Gibbs sampler and uncertainty estimation in geophysical inversion: Geophysical Prospecting, **44**, 313–350 doi: 10.1111/j.1365-2478.1996.tb00152.x.
Spikes, K., T. Mukerji, J. Dvorkin, and G. Mavko, 2008, Probabilistic seismic inversion based on rock-physics models: Geophysics, **72**, no. 5, R87–R97, doi: 10.1190/1.2760162.
Tarantola, A., 2005, Inverse problem theory: SIAM.
Tarantola, A., and B. Valette, 1982, Inverse problems = quest for information: Journal of Geophysics, **50**, 159–170.
Tromp, J., and R. Snieder, 1989, The reflection and transmission of plane P-and S-waves by a continuously stratified band: A new approach using invariant imbedding: Geophysical Journal International, **96**, 447–456, doi: 10.1111/j.1365-246X.1989.tb06006.x.
Ulrych, T. J., M. D. Sacchi, and A. Woodbury, 2001, A Bayes tour of inversion: A tutorial: Geophysics, **66**, 55–69, doi: 10.1190/1.1444923.